

Article

The Effects of Biofouling and Corrosion Products on Impressed Current Cathodic Protection System Design for Offshore Monopile Foundations

Caglar Erdogan  and Geoffrey Swain *

Center for Corrosion and Biofouling Control, Florida Institute of Technology, Melbourne, FL 32901, USA

* Correspondence: swain@fit.edu

Abstract: The robustness of the cathodic protection systems utilized for offshore wind monopile foundations depends on the surface condition of the steel as well as the environmental conditions. This study investigated how preexisting biofouling and corrosion products on vertical uncoated steel surfaces extending from the intertidal zone to the buried zone affected the cathodic protection requirements when impressed current cathodic protection (ICCP) was applied under tidal conditions. The comparative results between initially clean and previously fouled and corroded panel sets showed that the fouling and corrosion products increased both the initial and mean current densities. They also altered the composition, slowed the formation, and reduced the protective properties of cathodic chinks during nine weeks of deployment in seawater at Port Canaveral, Florida.

Keywords: steel foundations; offshore wind; cathodic protection; electrodeposited films; rust; bio-fouling



Citation: Erdogan, C.; Swain, G. The Effects of Biofouling and Corrosion Products on Impressed Current Cathodic Protection System Design for Offshore Monopile Foundations. *J. Mar. Sci. Eng.* **2022**, *10*, 1670. <https://doi.org/10.3390/jmse10111670>

Academic Editor: Erkan Oterkus

Received: 3 October 2022

Accepted: 19 October 2022

Published: 5 November 2022

Publisher's Note: MDPI stays neutral with regard to jurisdictional claims in published maps and institutional affiliations.



Copyright: © 2022 by the authors. Licensee MDPI, Basel, Switzerland. This article is an open access article distributed under the terms and conditions of the Creative Commons Attribution (CC BY) license (<https://creativecommons.org/licenses/by/4.0/>).

1. Introduction

Corrosion is one of the major factors that determine the service life of offshore wind foundations in the marine environment. Monopiles, large-diameter cylinder steel structures, are the preferred foundations in shallow water depths up to about 40 m. These dominate the existing structures in most lease areas due to costs and simplicity of design and fabrication [1,2]. Corrosion protection methods utilized for monopile foundations include corrosion allowance, coatings, and cathodic protection systems [3]. Coatings are optional for external and internal submerged surfaces [4], and these structures may not receive any cathodic protection for up to 2 years until the transition piece is installed where the sacrificial anodes are located [5]. This practice allows corrosion products to form and fouling organisms to become established on the surfaces before cathodic protection is applied. The ISO 24656:2022—Cathodic Protection of Offshore Wind Structures is the only standard that recommends immediate cathodic protection of offshore monopile foundations. Therefore, this study investigated how fouled and corroded vertical steel surfaces at different zones, including intertidal, submerged, and buried zones alter the cathodic protection design current densities under tidal cycles. The knowledge gained through this experiment may be utilized to advance the robustness and effectiveness of cathodic protection in the marine environment.

The fouling communities in marine environments are comprised of both micro- and macro-organisms. These communities may alter the corrosion dynamics at both the cathodes and anodes. The fouling established on steel surfaces may act as a barrier by limiting oxygen transfer to steel surfaces [6]. This causes the generation of both micro- and macro-galvanic cells due to the heterogeneous distribution of oxygen [6–9] and alters the conditions in the vicinity by establishing a source or a sink for chemical species [10–14]. The fouling causing localized and pitting corrosion [9,15–17] may result in local stress concentrations and reduce the fatigue life of offshore monopile foundations [4,18,19].

The accumulation of fouling on inactive anodes, for example, when they are incorporated with coating systems for corrosion prevention may alter their corrosion prevention properties. Swain et al. [20] reported that the increase in resistance and the reduction in the current output of idle Al-Zn-Hg sacrificial anodes was higher compared to working anodes due to marine growth. Rousseau et al. [21] reported that the fouling settlement reduced the effectiveness of a zinc anode utilized to keep the polarization potentials of a carbon steel structure at -1.0 V (Ag/AgCl). Hence, the anode was cleaned periodically to increase the anode current output. However, Blackwood et al. [22] reported that both Al and Zn anodes utilized to protect 316L SS performed similarly under heavy and light fouling conditions.

The biofouling community and the rust layer established on freely corroding steel surfaces cause ennoblement and influence corrosion rates [8,23–27]. The relationship between the corrosion of steel, cathodic protection and biofouling is shown in Figure 1. Guezennec et al. [11] concluded that the two eubacteria increased the cathodic current demands of X52 carbon steel samples as a result of the modification of calcium and magnesium ion balances on the surface. Eashwar et al. [28] investigated the effect of fouling on CP for mild steel, 304 stainless steel and 3004 aluminum alloy samples. They reported that the macro-fouling on steel surfaces polarized to -1.07 V (SCE) caused approximately 300 mV ennoblement and depolarized to -0.77 V and highlighted that the change in potential due to fouling could affect the CP system design and could cause underprotection. Dexter et al. [10] reported that the UNS G10180 carbon steel samples with biofilms required significantly higher cathodic corrosion currents (4.3–5.0 mA) compared to the clean samples (0.84–0.89 mA). Chen et al. [29] investigated the change in cathodic current densities when X70 carbon steel samples were immersed in a solution with and without biofilms. They concluded that the presence of biofilms decreased the potential of X70 steel and increased the current densities. Permeh et al. [30] concluded that the increased marine fouling on carbon steel surfaces increased the current densities required for cathodic polarization. Liduino et al. [31] reported an increase in cathodic current densities of AISI 1020 steel after samples were immersed in seawater for 28 days. However, the studies did not consider the effects of different corrosion zones and the effect of tides on current densities when fouling and corrosion products are present on steel surfaces.

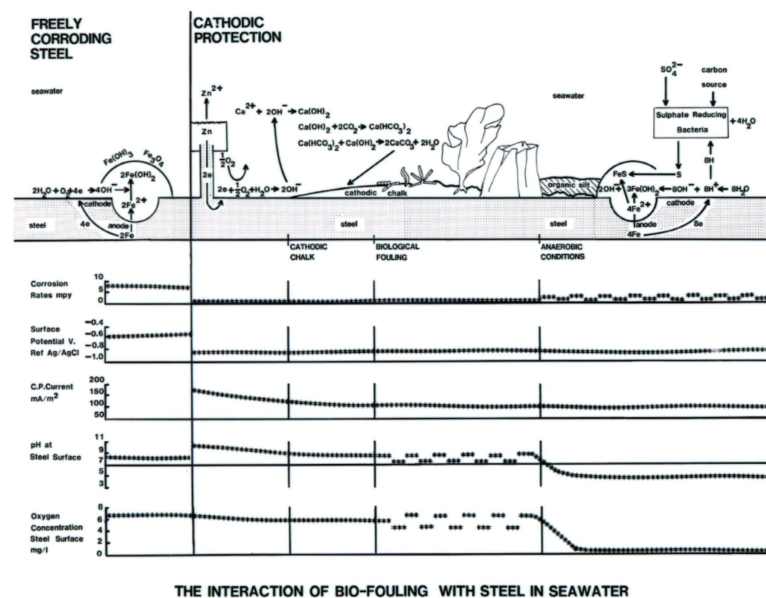


Figure 1. Interaction of biofouling with steel in seawater [32].

This study investigated the influence of biofouling and corrosion products on the cathodic current demands of previously fouled and corroded panels in seawater at Port Canaveral, FL. The steel panels were placed at the intertidal, submerged, and buried zones

in seawater, thus the influence of semidiurnal tides was also recorded. The continuity between each set of panels was provided by electrical connections. The polarization potentials, current flow between panels, and total current output from each ICCP system were collected and the fouling progression was monitored. The results were compared against a clean set of panels that had not been subjected to corrosion or biofouling.

2. Materials and Methods

2.1. Test Site and Environmental Conditions

The Center’s seawater test site is located at Port Canaveral, FL (28°24’30.93” N, 80°37’39.31” W). The data collection was performed for nine weeks from 7 October 2021 to 7 December 2021. The vertical layout of the panels was designed according to water depths and the semidiurnal tides. The predicted water depths at low and high tides were 3.70 m and 5.30 m, respectively (Figure 2) [33]. Temperature and salinity were recorded using YSI 30 conductivity meter and pH was recorded with an Onset HOBO MX2501 datalogger (Figure 3). The major ions in seawater at the test site are shown in Table 1.

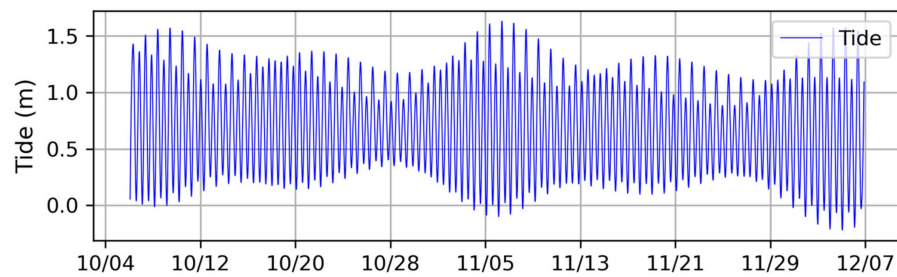


Figure 2. Tide cycle during the experiment.

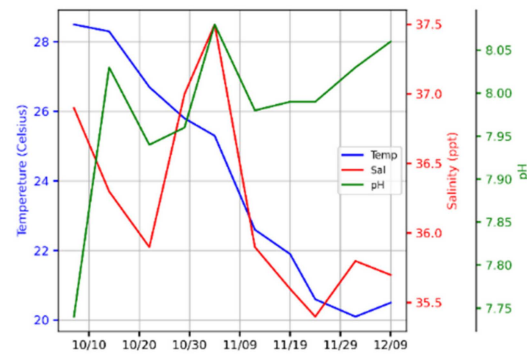


Figure 3. Temperature, salinity, and pH.

Table 1. Major ion concentrations in seawater during the experiment.

	mg/L in Seawater
Chloride [Cl ⁻]	19.91 ± 0.37
Sodium [Na ⁺]	11.06 ± 0.20
Sulfate [SO ₄ ²⁻]	2.79 ± 0.05
Magnesium [Mg ²⁺]	1.33 ± 0.02
Calcium [Ca ²⁺]	0.42 ± 0.01
Potassium [K ⁺]	0.40 ± 0.01

2.2. Materials and Experimental Setup

Two sets of A36 low carbon steel panels were used (Table 2). Each set consisted of five 300 mm by 150 mm panels with 3 mm thickness. Both sides of the steel panels were white

metal sandblasted according to SSPC-SP 5 (NACE No.1) by removing corrosion products, oxide layers, grease, and oil. The surface roughness of the panels was $25.3 \pm 2.2 \mu\text{m}$ (Mahr, Marsurf PS10, USA). The backs of the panels were coated with one layer of epoxy, a tie coat and a topcoat of Hempel, Hempaguard[®] X7, Denmark fouling control system to define the area exposed to corrosion and eliminate the weight increase due to biofouling. Two PVC frames were designed and built to allow one panel to be exposed to constant wetting and drying cycles while having a 110 cm distance between panels. Each set of panels was attached to a fixed PVC frame to have one panel (panel 1) in the intertidal zone and three panels (panels 2,3 and 4) in the submerged zone. The last panel (panel 5) was semi buried in the sediment (Figure 4). One set of panels was deployed in seawater at the test site for nine weeks prior to this experiment to allow for corrosion and the recruitment of biofouling (Figure 5).

Table 2. Composition of steel panels.

	wt%
Carbon [C]	0.25
Copper [Cu]	0.2
Iron [Fe]	rem
Manganese [Mn]	1.03
Phosphorus [P]	0.04
Silicon [Si]	0.28
Sulfur [S]	0.05

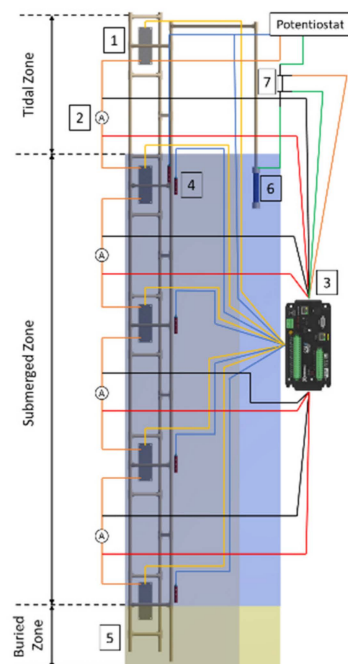


Figure 4. Experimental setup: (1) Steel Panel, (2) ZRA, (3) Datalogger, (4) Ag/AgCl Reference Electrode, (5) PVC Frame, (6) MMO Anode, (7) 1-Ohm Shunt.

On each frame, the electrical connection between panels was provided by 12 AWG wires 30 ft long. The current flow between panels was measured by using the channels of an ElectroSynthesis, Model 440, USA multichannel potentiostat as zero resistance ammeters (ZRAs). Silver/silver chloride seawater reference electrodes (Ag/AgCl) were used to measure the corrosion potentials of individual panels. The reference cells were placed in

perforated PVC housings which were coated with antifouling coating systems and filled with fiberglass wool to prevent influences of fouling during the experiment.

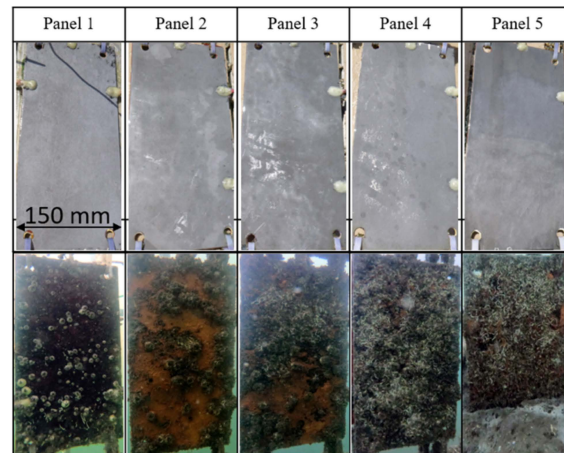


Figure 5. Clean (**top**) and previously fouled and corroded (**bottom**) panels.

The panels were cathodically protected, using ICCP, to a potential of -1.0 V (Ag/AgCl) measured at panel 2. This followed the DNV-RP-B401 recommended practice to increase the formation of cathodic chalks and reduce the current densities. The cathodic protection current was provided from a Thompson Electrochem, Ministat Precision, UK for the clean panels and a single channel of the Electrosynthesis, Model 440, USA multichannel potentiostat for the corroded and fouled panels. A 25 mm by 150 mm ribbon mesh mixed metal oxide (MMO) anode was used to apply the current to each set of steel panels. The anodes were aligned and placed 1 m away from Panel 2, the top panels in the submerged zone. The total current output from the ICCP systems for each set of panels was measured over a 1-Ohm shunt. The reference electrodes and the 1-Ohm shunts were connected to a Campbell Scientific, CR6 datalogger, USA and a Campbell Scientific, AM16/32B, USA relay multiplexer for data collection. The sampling rate for the data collection was every minute.

The panels were photographed underwater weekly for visual assessment of cathodic chalks, biofouling and corrosion products. The composition of cathodic chalks was analyzed by scanning electron microscopy (JEOL JSM-6380LV) with electron dispersive X-ray spectroscopy (EDAX Octane Elect EDS system with APEX software version 3.1). The samples were prepared with gold sputtering before the analysis. There were no replications for this pilot study in natural seawater due to the scale and the high number of sensors required.

3. Results and Discussion

The results are reported for both initially clean and previously fouled and corroded panels, and include the data from polarization potentials, electric current flows between panels, total current densities of ICCP systems, and the visual assessments of biofouling, corrosion products and cathodic chalks during and at the end of the experiment. The results for the panels on both racks are discussed in comparison to each other.

3.1. Polarization Potentials

The polarization potential selected for both sets of panels was -1.0 V (Ag/AgCl/seawater). Hartt [34] concluded that the cathodic chalks formed between the potentials -0.9 and -1.05 V (Ag/AgCl/seawater) create a less porous structure and help reduce the cathodic protection current densities. The potentials of the panels reached the design cathodic protection potentials approximately a week after immersion (Figure 6). Although the intertidal panels were polarized immediately to -1.0 V (Ag/AgCl/seawater), the polarization of clean panels took a couple of days longer compared to the previously fouled and corroded panels.

This was assumed to be due to the reduction of the total surface area by fouling and corrosion products which created a protective barrier [30]. The polarization of the bottom panel on each set was the slowest compared to the other panels due to IR drop [35].

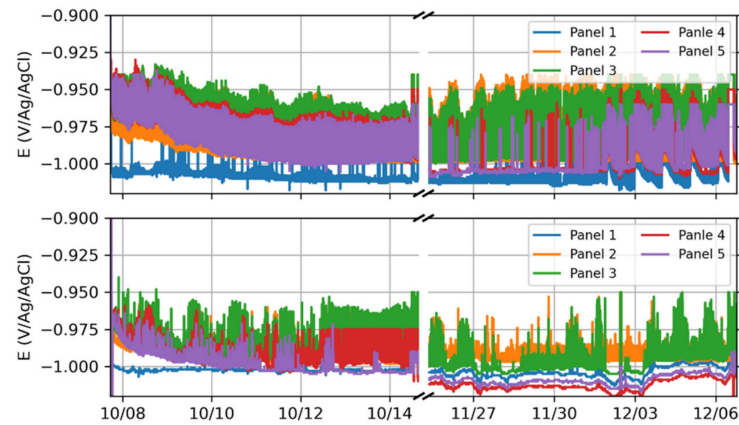


Figure 6. Polarization potentials: Clean (**top**) and previously fouled and corroded (**bottom**).

3.2. Cathodic Protection Current Densities

The cathodic protection current densities were normalized by dividing the amount of current impressed from each anode by the corresponding total steel area (m^2). The results showed that the current densities required to mitigate corrosion are highly dependent on the intertidal panels for both arrays. This was mainly due to the macro-galvanic cells formed as a result of the high partial pressure of oxygen generated during the semidiurnal tide cycles [7,8]. However, the increase in current densities was higher for the previously fouled and corroded panels when the intertidal panels were exposed to constant wetting and drying cycles [36]. The initial current density was estimated using the guidelines from the DNV recommended practice which states that it is the average current density until it attains a constant value. For the clean panel set was $175.5 \text{ mA}/m^2$, whereas it was $517.5 \text{ mA}/m^2$ for the previously fouled and corroded panels. This was due to biofouling and corrosion products causing ennoblement of the surface as well as delaying the formation of cathodic chalks that normally reduce the current densities [28,37,38].

The intertidal panels were constantly submerged during super high tides. This caused ICCP currents to converge approximately after two months of immersion. However, the divergence occurred when the intertidal panels started to experience wetting and drying cycles towards the end of the experiment (Figure 7). The mean current densities for the clean and the previously fouled and corroded panel sets were around $67 \text{ mA}/m^2$ and $115 \text{ mA}/m^2$, respectively.

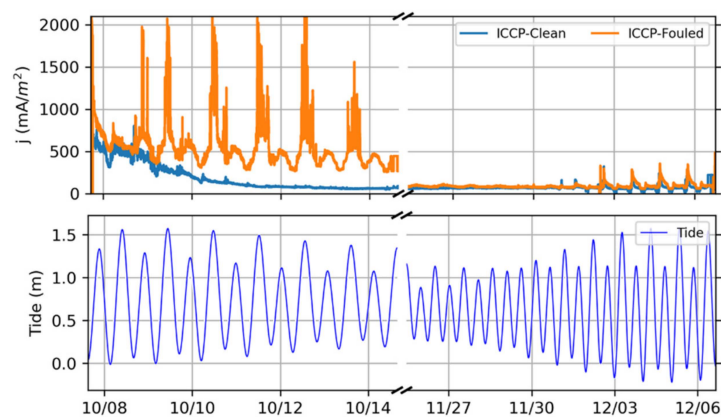


Figure 7. ICCP current density comparison: Clean vs. previously fouled and corroded (**top**) and tide (**bottom**).

3.3. Current Flow between Panels

The electric current flows measured over the zero resistance ammeters were used to measure the changes on panels that were constantly submerged and excluded the intertidal panel (panel 1). This demonstrates the differences caused by macro galvanic contributions of the steel in the intertidal zone. The current densities for the clean panels were higher in the beginning than the previously fouled and corroded panels (Figure 8). For example, the total current density after two days of immersion for the initially clean panels 2, 3, 4, and 5 was around 483 mA/m^2 , whereas it was 361 mA/m^2 for the previously fouled and corroded panels. This was due to both micro- and macro-fouling creating a barrier in the vicinity of the surface and blocking oxygen transfer to the surface [6]. Additionally, the corrosion products on the steel surface comprised of magnetite (Fe_3O_4), $\alpha\text{-FeOOH}$, and $\beta\text{-FeOOH}$ created a barrier with high resistance and reduced the current flow into the panels [39].

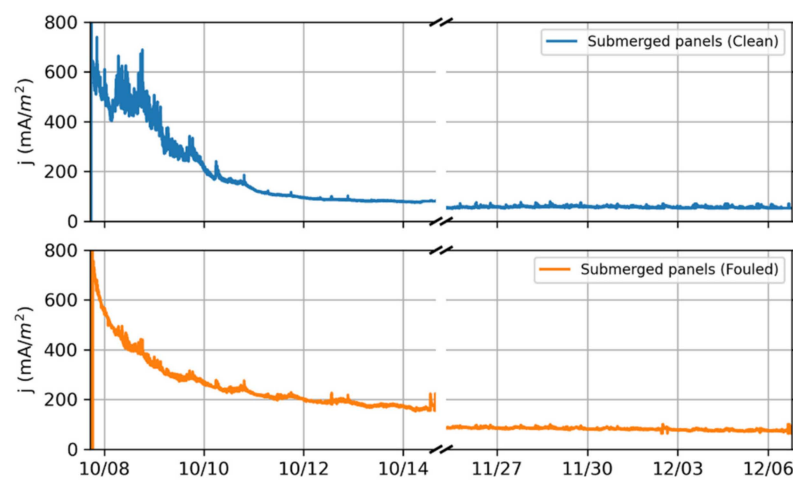


Figure 8. Current densities of constantly submerged panels: Clean (top) and previously fouled and corroded (bottom).

The current densities for the submerged clean panels decreased faster than the previously fouled and corroded panels and stabilized almost in five days of immersion (Figure 8). Although the initial current densities for previously fouled and corroded panels were low, it required almost a month for current densities to stabilize. The current densities for the fouled and corroded panels were higher than those measured for the clean panels even after the current densities were stabilized. For example, towards the end of the experiment the current density required for the clean panels was around 53 mA/m^2 , whereas it was around 83 mA/m^2 for the previously fouled and corroded panels. This was due to the formation of cathodic chalks, for example, calcium carbonates (CaCO_3) and magnesium hydroxides (Mg(OH)_2) on clean panels which created a protective layer and reduced the current densities required to prevent corrosion [16,33]. However, the cathodic chalks formed on the fouled and corroded panels were less protective due to their morphology being disrupted by the biofouling and corrosion products [28,36,37].

3.4. Fouling

The fouling on panels was assessed at the end of the experiment after a light cleaning. The results showed that the density of fouling organisms on an initially clean set of panels was higher than the previously fouled and corroded one, although the latter was immersed in seawater longer [40]. This was due to the stable cathodic chalk formation on the clean panels. The fouling on panel 1 of the initially clean set was less than the rest of the panels on that array since constant wetting and drying cycles reduced the fouling settlement rate [24]. The main macrofoulers on panels were tubeworms and barnacles. Initially clean panels had some encrusting bryozoans and tunicates on constantly submerged panels. The

previously fouled panels had some oysters (Figure 9). Scraping off the cathodic chalks and fouling from initially clean panels revealed that chalk formation and the settlement happened at the same time [41] and the areas under the barnacles were covered with dark corrosion products assuming that they were a thin layer of Fe(II)-based corrosion products with magnetite [42] (Figure 10).

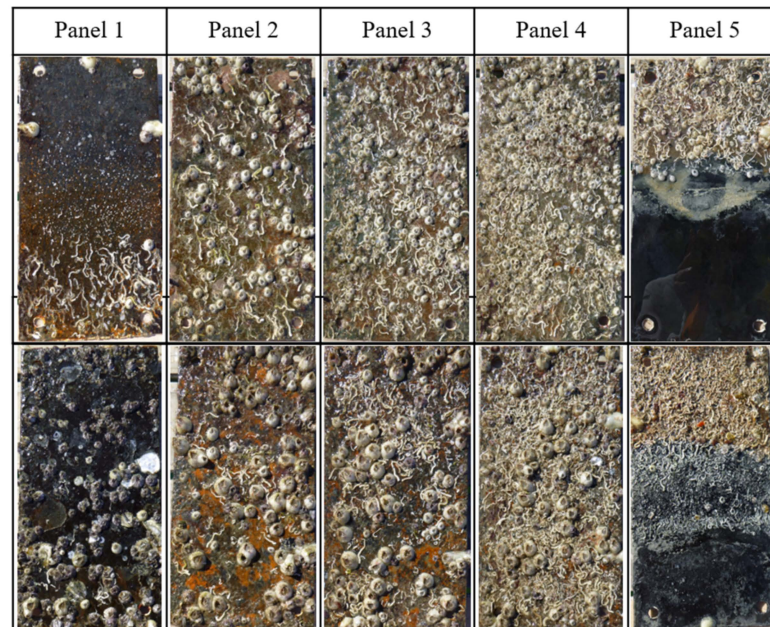


Figure 9. Final visual assessment of the initially clean (**top**) and the previously fouled and corroded (**bottom**) panels after light cleaning.



Figure 10. Condition of the initially clean panel after scraped off.

3.5. Corrosion, Cathodic Chalks and EDX Analysis

The corrosion and cathodic chalks formed on initially clean and previously fouled and corroded panels showed visual differences. The clean panels showed no signs of corrosion except the intertidal panel since they were completely covered with cathodic chalks. The panels 2, 3, and 4 of the previously fouled and corroded array had bright orange areas after cathodic protection with an ICCP system for nine weeks (Figure 11). The buried areas for both arrays were free of corrosion and covered with a thin layer of chalk.

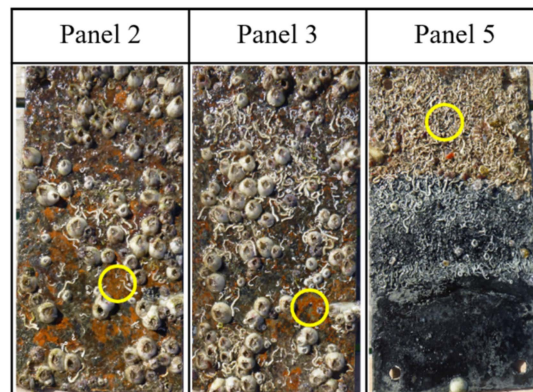


Figure 11. Areas analyzed with EDX.

The products on the bright orange areas on previously fouled and corroded panels were analyzed with EDX to determine their composition. The EDX analyses showed that the cathodic chalks formed at these areas were infused with initially present corrosion products and contained Fe element in addition to Ca and Mg. The sample taken from the buried zone of panel 5 was mainly Ca and Mg [13,27], however there was no Fe present (Figure 12). This may have been due to the iron being held in the black iron oxide films which were not removed during sampling.

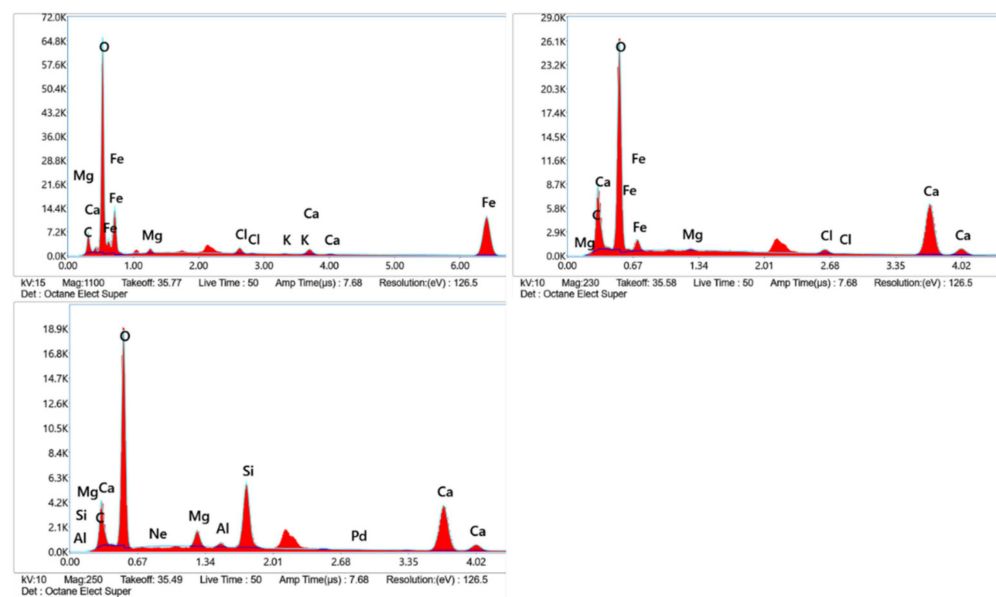


Figure 12. EDX analysis of previously fouled and corroded panels: Panel 2 (top left), Panel 3 (top right), and Panel 5 (bottom left).

The data collected for this study was specific to the environmental conditions at Port Canaveral, FL between 7 October 2021 and 7 December 2021. It was also specific to the condition of previously fouled and corroded panels. The amount of fouling and corrosion products was a result of the deployment in seawater at Port Canaveral, FL for nine weeks between 5 August 2021 and 7 October 2021. The ratio of fouling and corrosion products may alter the results presented in this paper. Therefore, it is recommended to deploy steel panels and perform similar experiments at locations with different environmental conditions.

4. Conclusions

The fouling and corrosion products established on offshore monopile foundations between deployment in marine environments and receiving any protection may alter the

design requirements of cathodic protection systems. These systems can be optimized and designed more efficiently by understanding the influence of fouling and corrosion products under dynamic conditions due to tidal cycles.

This study demonstrated that the fouling and corrosion products on vertical uncoated steel surfaces in seawater extending from the intertidal zone to the buried zone increased the cathodic protection current densities. The initial current densities for the clean panels and the previously fouled and corroded panels were 175.5 mA/m² and 517.5 mA/m², respectively. The mean current density was 67 mA/m² for the clean panels and it was 115 mA/m² for the previously fouled and corroded panels. The current density values became closer during constant immersion due to super high tides. However, wetting and drying cycles towards the end of the experiment caused higher fluctuations of current densities for the previously fouled and corroded panels.

The initial current density for the clean panels (489 mA/m²) below the waterline was higher than the previously fouled and corroded panels (361 mA/m²). However, due to the immediate formation of stable cathodic chalks on the clean panels, the currents decreased faster. The current densities for both arrays became stable during the experiment, and they were lower for the clean panels (53 mA/m²) than the previously fouled and corroded panels (83 mA/m²).

The visual assessments showed no signs of corrosion and a more diverse fouling community on the clean panels with an ICCP system below the waterline. The fouled and corroded panels had areas that were bright orange in the submerged zone. The EDX analysis of the samples from these areas showed that the cathodic chalks included Fe as well as Ca and Mg. This demonstrated that the fouling as well as the corrosion products changed the composition of cathodic chalks.

The fouling and corrosion products on uncoated steel surfaces have been shown to increase the current demand for cathodic protection systems and alter the composition of cathodic chalks while reducing their protection properties. This study highlights the benefits of applying cathodic protection to offshore monopiles immediately after they are deployed in seawater.

Author Contributions: Conceptualization, C.E. and G.S.; Writing—Original Draft, C.E.; Formal analysis, C.E.; Investigation, C.E.; Methodology, C.E. and G.S.; Project administration, C.E.; Supervision, G.S.; Visualization, C.E.; Writing—Review and Editing, C.E. and G.S. All authors have read and agreed to the published version of the manuscript.

Funding: This research received no external funding.

Institutional Review Board Statement: Not applicable.

Informed Consent Statement: Not applicable.

Data Availability Statement: The data that support the findings of this study are available from the corresponding author upon request.

Acknowledgments: We would like to acknowledge the Office of Naval Research [grant number N00014-20-1-2243] for access to the sea water test site they support at the Center for Corrosion and Biofouling Control, Port Canaveral, Florida. We offer special thanks to Dan Kuchma from the Tufts University and the Bureau of Ocean Energy Management for their indirect support for this project.

Conflicts of Interest: The authors declare no conflict of interest.

References

1. Gupta, B.K.; Basu, D. Offshore wind turbine monopile foundations: Design perspectives. *Ocean Eng.* **2020**, *213*, 107514. [[CrossRef](#)]
2. Bisoi, S.; Haldar, S. Dynamic analysis of offshore wind turbine in clay considering soil–monopile–tower interaction. *Soil Dyn. Earthq. Eng.* **2014**, *63*, 19–35. [[CrossRef](#)]
3. Erdogan, C.; Swain, G. Conceptual Sacrificial Anode Cathodic Protection Design for offshore wind monopiles. *Ocean Eng.* **2021**, *235*, 109339. [[CrossRef](#)]
4. Price, S.J.; Figueira, R.B. Corrosion Protection Systems and Fatigue Corrosion in Offshore Wind Structures: Current Status and Future Perspectives. *Coatings* **2017**, *7*, 25. [[CrossRef](#)]

5. DNVGL. *Recommended practice—Corrosion Protection for Wind Turbines*; DNVGL-RP-0416; DNVGL: Bærum, Norway, 2016.
6. De Brito, L.V.R.; Coutinho, R.; Cavalcanti, E.H.S.; Benchimol, M. The influence of macrofouling on the corrosion behaviour of API 5L X65 carbon steel. *Biofouling* **2007**, *23*, 193–201. [[CrossRef](#)]
7. Wyatt, B.S.; Preston, J.; Jacob, W.R. Cathodic Protection of Offshore Renewable Energy Infrastructure. In Proceedings of the Eurocorr Conference, Brussels, Belgium, 7–11 September 2020.
8. Erdogan, C.; Swain, G. The effect of macro-galvanic cells on corrosion and impressed current cathodic protection for offshore monopile steel structures. *Ocean Eng.* **2022**, *265*, 112575. [[CrossRef](#)]
9. Cui, Z.; Chen, S.; Dou, Y.; Han, S.; Wang, L.; Man, C.; Wang, X.; Chen, S.; Cheng, Y.F.; Li, X. Passivation behavior and surface chemistry of 2507 super duplex stainless steel in artificial seawater: Influence of dissolved oxygen and pH. *Corros. Sci.* **2019**, *150*, 218–234. [[CrossRef](#)]
10. Dexter, S.C.; Lafontaine, J.P. Effect of Natural Marine Biofilms on Galvanic Corrosion. *Corrosion* **1998**, *54*, 851–861. [[CrossRef](#)]
11. Guezennec, J.; Edowling, N.J.; Bullen, J.; White, D.C. Relationship between bacterial colonization and cathodic current density associated with mild steel surfaces. *Biofouling* **1994**, *8*, 133–146. [[CrossRef](#)]
12. Perme, S.; Lau, K. Identification of steel corrosion associated with sulfate-reducing bacteria by electrochemical noise technique. *Mater. Corros.* **2022**. [[CrossRef](#)]
13. Carré, C.; Zanibellato, A.; Jeannin, M.; Sabot, R.; Gunkel-Grillon, P.; Serres, A. Electrochemical calcareous deposition in seawater. A review. *Environ. Chem. Lett.* **2020**, *18*, 1193–1208. [[CrossRef](#)]
14. Little, B.J.; Blackwood, D.J.; Hinks, J.; Lauro, F.M.; Marsili, E.; Okamoto, A.; Rice, S.A.; Wade, S.A.; Flemming, H.C. Microbially Influenced Corrosion—Any Progress? *Corros. Sci.* **2020**, *170*, 108641. [[CrossRef](#)]
15. Lv, M.; Du, M. A review: Microbiologically influenced corrosion and the effect of cathodic polarization on typical bacteria. *Rev. Environ. Sci. Bio/Technol.* **2018**, *17*, 431–446. [[CrossRef](#)]
16. Thompson, A.A.; Wood, J.L.; Palombo, E.A.; Green, W.K.; Wade, S.A. From laboratory tests to field trials: A review of cathodic protection and microbially influenced corrosion. *Biofouling* **2022**, *38*, 298–320. [[CrossRef](#)]
17. Tian, H.; Xin, J.; Li, Y.; Wang, X.; Cui, Z. Combined effect of cathodic potential and sulfur species on calcareous deposition, hydrogen permeation, and hydrogen embrittlement of a low carbon bainite steel in artificial seawater. *Corros. Sci.* **2019**, *158*, 108089. [[CrossRef](#)]
18. Shojai, S.; Schaumann, P.; Braun, M.; Ehlers, S. Influence of pitting corrosion on the fatigue strength of offshore steel structures based on 3D surface scans. *Int. J. Fatigue* **2022**, *164*, 107128. [[CrossRef](#)]
19. Khodabux, W.; Liao, C.; Brennan, F. Characterisation of pitting corrosion for inner section of offshore wind foundation using laser scanning. *Ocean Eng.* **2021**, *230*, 109079. [[CrossRef](#)]
20. Swain, G.W.; Patrick-Maxwell, J. The Effect of Biofouling on the Performance of Al-Zn-Hg Sacrificial Anodes. *Corrosion* **1990**, *46*, 256–260. [[CrossRef](#)]
21. Rousseau, C.; Baraud, F.; Leleyter, L.; Jeannin, M.; Gil, O. Calcareous deposit formed under cathodic protection in the presence of natural marine sediments: A 12 month experiment. *Corros. Sci.* **2010**, *52*, 2206–2218. [[CrossRef](#)]
22. Blackwood, D.J.; Lim, C.S.; Teo, S.L. Influence of fouling on the efficiency of sacrificial anodes in providing cathodic protection in Southeast Asian tropical seawater. *Biofouling* **2010**, *26*, 779–785. [[CrossRef](#)]
23. Rajala, P.; Sohlberg, E.; Priha, O.; Tsitko, I.; Väisänen, H.; Tausa, M.; Carpén, L. Biofouling on Coated Carbon Steel in Cooling Water Cycles Using Brackish Seawater. *J. Mar. Sci. Eng.* **2016**, *4*, 74. [[CrossRef](#)]
24. Daille, L.K.; Aguirre, J.; Fischer, D.; Galarce, C.; Armijo, F.; Pizarro, G.E.; Walczak, M.; De la Iglesia, R.; Vargas, I.T. Effect of Tidal Cycles on Bacterial Biofilm Formation and Biocorrosion of Stainless Steel AISI 316L. *J. Mar. Sci. Eng.* **2020**, *8*, 124. [[CrossRef](#)]
25. Eashwar, M.; Subramanian, G.; Palanichamy, S.; Rajagopal, G.; Madhu, S.; Kamaraj, P. Cathodic behaviour of stainless steel in coastal Indian seawater: Calcareous deposits overwhelm biofilms. *Biofouling* **2009**, *25*, 191–201. [[CrossRef](#)] [[PubMed](#)]
26. Choudhary, S.; Garg, A.; Mondal, K. Relation Between Open Circuit Potential and Polarization Resistance with Rust and Corrosion Monitoring of Mild Steel. *J. Mater. Eng. Perform.* **2016**, *25*, 2969–2976. [[CrossRef](#)]
27. Wang, W.; Li, W.; Song, L.-Y.; Fan, W.-J.; Liu, X.-J.; Zheng, H. Numerical simulation and re-design optimization of impressed current cathodic protection for an offshore platform with biofouling in seawater. *Mater. Corros.* **2018**, *69*, 239–250. [[CrossRef](#)]
28. Eashwar, M.; Subramanian, G.; Chandrasekaran, P.; Manickam, S.T.; Maruthamuthu, S.; Balakrishnan, K. The interrelation of cathodic protection and marine macrofouling. *Biofouling* **1995**, *8*, 303–312. [[CrossRef](#)]
29. Chen, X.; Wang, G.; Gao, F.; Wang, Y.; He, C. Effects of sulphate-reducing bacteria on crevice corrosion in X70 pipeline steel under disbanded coatings. *Corros. Sci.* **2015**, *101*, 1–11. [[CrossRef](#)]
30. Perme, S.; Lau, K.; Boan, M.E.; Tansel, B.; Duncan, M. Cathodic Polarization Behavior of Steel with Different Marine Fouling Morphologies on Submerged Bridge Elements with Cathodic Protection. *J. Mater. Civ. Eng.* **2020**, *32*, 04020184. [[CrossRef](#)]
31. Liduino, V.; Galvão, M.; Brasil, S.; Sérvulo, E. SRB-mediated corrosion of marine submerged AISI 1020 steel under impressed current cathodic protection. *Colloids Surf. B Biointerfaces* **2021**, *202*, 111701. [[CrossRef](#)]
32. Swain, G. *Corrosion and Types of Corrosion—Protection of Marine Materials*. Center for Corrosion and Biofouling Control; Internal Report; Florida Institute of Technology: Melbourne, FL, USA, 2022.
33. NOAA Tide Predictions—8721604 Trident Pier, Port Canaveral, FL. Available online: <https://tidesandcurrents.noaa.gov/noaatidepredictions.html?id=8721604> (accessed on 7 January 2021).

34. Hartt, W. 2012 Frank Newman Speller Award: Cathodic Protection of Offshore Structures—History and Current Status. *Corrosion* **2012**, *68*, 1063–1075. [[CrossRef](#)]
35. Revie, R.W.; Uhlig, H.H. *Corrosion and Corrosion Control: An Introduction to Corrosion Science and Engineering*, 4th ed.; John Wiley & Sons, Inc.: Hoboken, NJ, USA, 2008; ISBN 9780470277270.
36. De Romero, M.; de Rincón, O.; Ocando, L. Cathodic Protection Efficiency in the Presence of SRB: State of the Art. In Proceedings of the NACE—International Corrosion Conference Series, Atlanta, GA, USA, 22–26 March 2009.
37. Dexter, S.C.; Lin, S.H. Effect of Marine Bacteria on Calcareous Deposition. *Mater. Perform.* **1991**, *30*, 16–21.
38. Dexter, S.C.; Lin, S.-H. Effect of marine biofilms on cathodic protection. *Int. Biodeterior. Biodegrad.* **1992**, *29*, 231–249. [[CrossRef](#)]
39. Wang, H.-H.; Du, M. Corrosion Behavior of a Low-Carbon Steel in Simulated Marine Splash Zone. *Acta Met. Sin. (Engl. Lett.)* **2017**, *30*, 585–593. [[CrossRef](#)]
40. Zhang, J.; Yu, Z.; Zhao, X.; Lan, X.; Wang, J.; Lv, X.; Zhang, C.; Duan, J.; Hou, B. The Interaction of Biofoulants and Calcareous Deposits on Corrosion Performance of Q235 in Seawater. *Materials* **2020**, *13*, 850. [[CrossRef](#)] [[PubMed](#)]
41. Hernandez, G.; Hartl, W.; Videla, H. Marine Biofilms and their Influence on Cathodic Protection: A Literature Survey. *Corros. Rev.* **1994**, *12*, 29–40. [[CrossRef](#)]
42. Refait, P.; Grolleau, A.-M.; Jeannin, M.; Rémazeilles, C.; Sabot, R. Corrosion of Carbon Steel in Marine Environments: Role of the Corrosion Product Layer. *Corros. Mater. Degrad.* **2020**, *1*, 198–218. [[CrossRef](#)]